Weather Clim. Dynam., 7, 2267–2276, 2026
https://doi.org/10.5194/wcd-7-2267-2026
© Author(s) 2026. This work is distributed under
the Creative Commons Attribution 4.0 License.

Weather and Climate Dynamics
Open Access
EGU

A new simple and accurate measure of baroclinicity in the North Atlantic storm track

Rhiannon Biddiscombe[1], **Maarten Ambaum**[1], **and Ben Harvey**[1,2]

[1]Department of Meteorology, University of Reading, Reading, UK
[2]National Centre for Atmospheric Science, University of Reading, Reading, UK

Correspondence: Rhiannon Biddiscombe (r.biddiscombe@pgr.reading.ac.uk)

Received: 27 May 2026 – Discussion started: 11 June 2026
Revised: 11 November 2026 – Accepted: 11 November 2026 – Published: 23 November 2026

Abstract. Baroclinicity is the measure of baroclinic growth rate in the midlatitude storm tracks. Spatially, it defines the genesis region of the storm track and, temporally, it sets the growth rate of storms in the storm track. Baroclinicity can be quantified with the Eady growth rate, which is proportional to the vertical shear of the zonal wind. This can alternatively be expressed as a meridional gradient of dry entropy via thermal wind balance. Both expressions of the Eady growth rate are equally valid given their derivation under the quasi-geostrophic approximations in which thermal wind balance is assumed. With a focus on the North Atlantic winter storm track, we demonstrate that variability in lower-tropospheric baroclinicity, averaged over a region encompassing the storm track, is determined almost entirely by lower-tropospheric dry entropy on the north edge of the storm track, with decreases in entropy on the north edge corresponding to increases in baroclinicity. We use physical arguments as well as a linear regression to relate storm track baroclinicity to the mean dry entropy to the north of the storm track, demonstrating that variability in area mean baroclinicity of the storm track is mainly determined by processes on its poleward side, rather than by local-scale internal processes within the storm track itself. It also provides a much simplified physical picture to accurately describe the dynamical budget of baroclinicity in the North Atlantic storm track.

1 Introduction

The development of cyclones in the storm tracks is enabled by the presence of upstream regions of high baroclinicity (Blackmon et al., 1977; Simmons and Hoskins, 1979). These pools of high baroclinicity act as fuel for the growth of cyclones, which erode baroclinicity as they redistribute heat poleward and reduce the potential for the development of new systems (Blackmon et al., 1977; Ambaum and Novak, 2014). When eddy activity in the storm track is weak, the strengthening of horizontal temperature gradients is enabled, restoring baroclinicity and making the storm track again favourable to the development of cyclones (Novak et al., 2015).

The Eady model is a simplified quasi-geostrophic model which captures the key physics of baroclinic instability, and from it emerges the Eady growth rate which characterises the rate of growth of the fastest growing mode in the Eady model and is generally considered a good measure of observed eddy growth rate, even for more complex vertical profiles than in the original model setup (Eady, 1949; Lindzen and Farrell, 1980). While the Eady growth rate typically depends on vertical shear of the zonal wind, it can be rearranged to a number of equally valid expressions under the assumptions of quasi-geostrophy.

A restorative mechanism for baroclinicity necessarily exists since the storm tracks are persistent features of the winter mid-latitudes (Hoskins and Valdes, 1990), which can be characterised in that it leads to steeper isentropic surfaces. Papritz and Spengler (2015) utilise a framework based on the slope of isentropes, where steeper slopes are indicative of favourable conditions for the development of cyclones, to analyse the evolution of baroclinicity within the storm tracks. In this perspective, latent heating acts significantly to maintain baroclinicity in the storm tracks. While this framework characterises well local features and their contribution to the generation of baroclinic eddies, a physical understanding of

baroclinicity and baroclinic instability depends on a larger-scale perspective in which the unstable mode of a baroclinic wave produces strong vorticity anomalies.

While baroclinicity may be calculated for all length scales, its relevance to the baroclinic growth rate is only meaningful on the scale of the fastest growing baroclinic waves. We interpret baroclinicity through the Eady growth rate to be the timescale for growth of these baroclinic wave modes, with the fastest growing modes typically having zonal wavenumbers 6–8, while in comparison the higher wavenumbers have reduced growth rates (Bretherton, 1966; Valdes and Hoskins, 1988). The baroclinically active interaction between the temperature gradients and the eddies therefore happens on these spatial scales, justifying the use of area mean baroclinicity as the dynamically relevant measure of baroclinic growth (Lorenz, 1955; James, 1994; Schemm and Rivière, 2019). While localised diabatic effects appear to facilitate cyclone intensification rates, cyclone clustering and other synoptic-scale features (Binder et al., 2016; Weijenborg and Spengler, 2020), it is not clear to what extent the persistence of horizontal temperature gradients is diabatically forced in the same way.

The role of diabatic effects can be contrasted with a more dynamical perspective such as Pinto et al. (2014), in which patterns in the eddy-driven jet and Rossby wave-breaking are linked to cyclone clustering, but here it is also not clear to what extent the observed large-scale Rossby wave breaking drives clustering or mainly diagnoses the concomitant high eddy activity.

The simulated storm tracks have some hard to mitigate biases, both in forecasting context (Rodwell et al., 2013) as well as climate context (Zappa et al., 2013), generally associated with too zonal eddy driven jets. We want to better understand the dynamics of baroclinicity itself to make progress on these issues. We propose to reformulate area mean baroclinicity in the North Atlantic (N. Atlantic) to a simple but accurate description in terms of mean dry entropy at the north edge of the storm track genesis region, demonstrating that this characterises well synoptic time-scale variability in the storm track, and indicating that this variability is not determined by detailed processes within the storm track itself.

2 Eady growth rate and thermal wind balance

In this study we use two-hourly reanalysis data for December, January, and February from ERA5 (Hersbach et al., 2020), starting from December 1991 and ending in February of 2021. Our focus is on the lower free troposphere as this is the height where baroclinicity is relevant to the baroclinic growth of cyclones, so we consider the pressure level range 800 to 750 hPa. To study baroclinicity in the N. Atlantic storm track we use a 0.25° horizontal grid covering the region 30 to 50° N and 30 to 80° W as illustrated by the green box in Fig. 1.

The Eady growth rate is usually defined as

$$\sigma_u = 0.31 \frac{|f|}{N} \frac{\partial u}{\partial z} \tag{1}$$

where f is the Coriolis parameter, N is the Brunt Väisälä frequency, and $\partial u/\partial z$ is the vertical shear of the zonal wind. For the southern hemisphere a minus-sign would be introduced in this equation. Here, the subscript u refers to the measure's dependence on vertical wind shear. The Brunt Väisälä frequency is

$$N = \left(\frac{g}{\theta}\frac{\partial \theta}{\partial z}\right)^{1/2} = \left(\frac{g}{c_p}\frac{\partial s}{\partial z}\right)^{1/2}, \tag{2}$$

where g is acceleration due to gravity and θ is potential temperature, and we introduce dry specific entropy s for an ideal gas, which depends on temperature and pressure as

$$\mathrm{d}s = c_p \frac{\mathrm{d}T}{T} - R\frac{\mathrm{d}p}{p}. \tag{3}$$

In the quasigeostrophic context the two expressions of N given in Eq. (2) are equivalent.

Using the thermal wind relation, σ_u can be rearranged in terms of a gradient in dry specific entropy, $\partial s/\partial y$. Because the thermal wind relation is not often considered in height coordinates (usually pressure or log-pressure coordinates are used) we write this out explicitly here, for a pressure level of 775 hPa in the middle of the range used for Eq. (1). We begin with geostrophic balance in pressure coordinates, considering only the zonal wind u and using Cartesian coordinates

$$fu = -\left(\frac{\partial \Phi}{\partial y}\right)_p, \tag{4}$$

where Φ is geopotential (Hoskins and James, 2014). Taking the vertical (pressure) derivative then leads to thermal wind balance in pressure coordinates.

$$f\frac{\partial u}{\partial p} = \frac{R}{p}\left(\frac{\partial T}{\partial y}\right)_p. \tag{5}$$

The subscript p indicates that the meridional derivative is taken at constant pressure. We used hydrostatic balance in pressure coordinates $(\partial\Phi/\partial p) = -1/\rho = -RT/p$ and the ideal gas law as relevant to the Eady model.

Hydrostatic balance also allows us to locally map pressure derivatives to height derivatives according to

$$\mathrm{d}\ln p = -\frac{g}{RT}\mathrm{d}z. \tag{6}$$

From this we can construct the relevant form of thermal wind balance

$$f\frac{\partial u}{\partial z} = -\frac{g}{T}\left(\frac{\partial T}{\partial y}\right)_p = -\frac{g}{c_p}\left(\frac{\partial s}{\partial y}\right)_p, \tag{7}$$

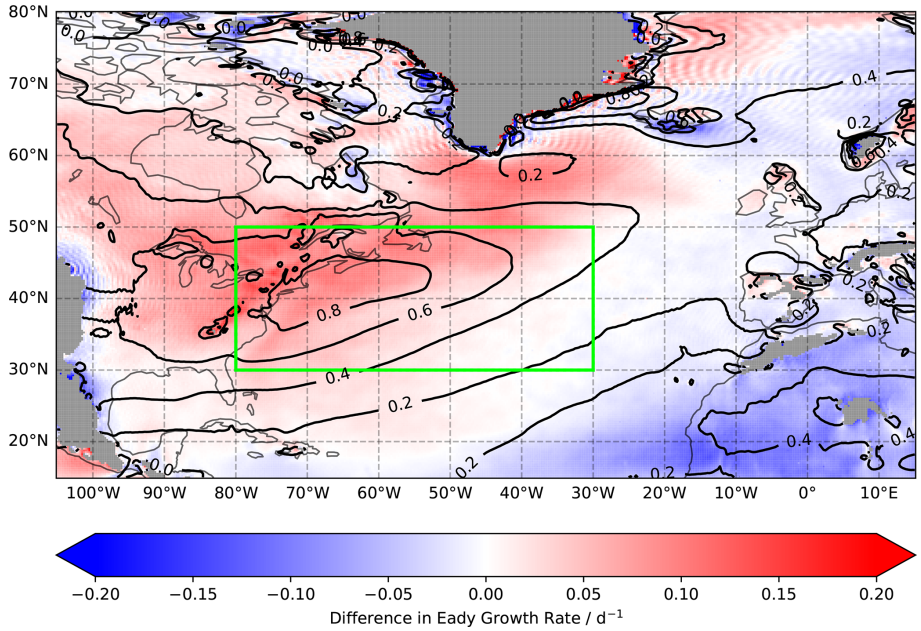

Figure 1. Comparison of forms of the Eady growth rate, σ_u (Eq. 1) and σ_s (Eq. 8). Contours show a 30 winter (1991–2021; DJF) climatological mean of σ_s in units of d^{-1} at 775 hPa. Colours show the climatological mean difference $\sigma_s - \sigma_u$ (i.e. σ_s is larger where values are positive). Stability N is calculated using Eq. (2) at 775 hPa at each grid point, with the derivative computed as a finite difference between 750 and 800 hPa. Surface heights above 1 km are masked in grey. The region commonly used in our analysis, 30 to 50° N, 30 to 80° W, is outlined in green.

where we are again considering dry entropy for an ideal gas, s, as it is more easily interpreted and evaluated.

Using this form of the thermal wind relation we can express baroclinicity in terms of the meridional gradient of dry entropy,

$$\sigma_s = -0.31 \frac{g}{c_p N} \left(\frac{\partial s}{\partial y} \right)_p . \tag{8}$$

Here, the subscript s refers to the measure's dependence on dry entropy. The sign of this equation is relevant for the northern hemisphere; for the southern hemisphere the minus-sign is removed. Note again that the meridional derivative of entropy is taken at constant pressure, allowing computation of the Eady growth rate using data at a single pressure level and without using vertical finite differences. In this expression we can treat stability, N, as either constant on a given pressure level or varying calculated with Eq. (2).

The rewritten version in Eq. (8) has the same level of validity as the more commonly encountered form from Eq. (1). The quasi-geostrophic model that defines the Eady growth rate as the relevant growth rate for baroclinic eddies is both geostrophic and hydrostatic, so in that context the two forms are equivalent.

Comparing these two forms of Eady growth rate, σ_u and σ_s, in reanalysis data, Fig. 1 shows the difference of 30 winter (DJF) climatologies centered on 775 hPa over the N. Atlantic in ERA5, where stability is calculated as Eq. (2). Within the storm track σ_s is found to be greater than σ_u, with the opposite being true over N. Africa. These match approximately the positions of the climatological low and high pressure regions associated with the N. Atlantic storm track.

Gradient wind balance gives a plausible explanation for these differences, as the wind about a low pressure system will be *subgeostrophic*, meaning an outward centrifugal force allows consistently slower speeds than the geostrophic wind, with faster *supergeostrophic* winds about a high pressure system. This suggests that around a climatological low σ_u is smaller than σ_s and vice versa around a climatological high. Assuming thermal wind balance, σ_u and σ_s are equal, so the differences between them are the result of ageostrophic effects and as such would not contribute to the quantification of baroclinic growth in a quasi-geostrophic context.

The Eady growth rate from Eq. (1), σ_u, features a diurnal cycle which does not appear in σ_s, a consequence of the top of the boundary layer increasing and decreasing in height from day to night (Marcheggiani and Ambaum, 2020). During the day, the top of the boundary layer raises and frictional effects result in a slowing of the wind, meaning vertical wind shear in the lower troposphere increases. This effect is more pronounced over land than ocean and contributes small, high frequency numerical changes that don't represent meaningful differences in the growth rate of baroclinic instabilities. Since our calculation of baroclinicity with Eq. (8) is mainly dependent on a single pressure level, the pressure at which we calculate $\partial s/\partial y$, it does not share this issue. To better

Table 1. Mean and standard deviation for different forms of the Eady growth rate. σ_u, σ_s, and σ_f are 30 to 50° N, 30 to 80° W area mean representations of Eqs. (1), (8), and (11), while σ_G uses a latitude-longitude mean over the same region, and is calculated using Eq. (12), and σ_n and σ_{south} are based on the linear regressions described in Eq. (13), which uses only data at one latitude and pressure level.

	Mean (d^{-1})	Standard Deviation (d^{-1})
σ_u (vertical wind shear)	0.53	0.149
σ_s (meridional entropy gradient)	0.54	0.150
σ_f (σ_s, fixed N)	0.54	0.152
σ_G (σ_f, not area mean)	0.55	0.159
σ_n (50° N entropy)	0.55	0.151
σ_south (30° N entropy)	0.55	0.070

compare the two fields, a 24 h running mean filter is hereafter applied to σ_u.

In this work we primarily consider area averaged baroclinicity in the region 30 to 50° N, 30 to 80° W, outlined by the green box in Fig. 1. This region is chosen because it contains the climatological maxima of both baroclinicity and meridional heat flux in the N. Atlantic storm track (Hoskins and Valdes, 1990). This upstream portion of the storm track is anchored in position by the land sea temperature contrast and strong sea surface temperature gradients of the region, making a fixed sampling region suitable (Hotta and Nakamura, 2011; Novak et al., 2015).

Figure 2a compares two-hourly area mean baroclinicity in the N. Atlantic storm track region over 30 winters calculated as σ_u and σ_s to demonstrate that the variability of these expressions are comparable. The mean and standard deviation for σ_u are 0.53 and 0.149 d^{-1} respectively, the mean and standard deviation for σ_s are 0.54 and 0.150 d^{-1}, and the Pearson correlation coefficient between them is 0.91, meaning their common variance is 83 % and their minimum uncertainty variance is therefore 17 %. Mean, standard deviation, and correlations for each formulation of σ are found in Tables 1 and 2.

While there are differences in values between σ_u and σ_s, both are valid expressions of the Eady growth rate since their applicability is only defined in the quasi-geostrophic framework, where the two expressions are equivalent. The similarity in variability of these measures of baroclinicity further validates using σ_s to express the Eady growth rate in the real atmosphere.

Up to this point we have considered N to be a varying field calculated between 750 and 800 hPa. The Brunt Väisälä frequency is commonly computed locally like this, however, since the Eady growth rate arises from quasi-geostrophic dynamics where N is a fixed parameter, constant in time and across surfaces of constant pressure, there is a theoretical justification to treat N as a given constant on a pressure level. To justify this approach in practice, we now show that the role of local variability in N, or more specifically $1/N$, in the Eady growth rate is small compared to contributions from the horizontal temperature gradients.

To treat $1/N$ as a parameter we need first to find its optimum value. This is not the same as calculating mean N for our region and period, rather we use a least squares fit between σ_s, where σ_s is calculated with Eq. (8), and $N \cdot \sigma_s$, removing stability from the denominator of Eq. (8), in order to find the best fit value, $1/N_0$. This method gives the optimum value of N at 775 hPa as $N_0 = 0.01484\,\mathrm{s}^{-1}$. Considering stability to be fixed, we then express the Eady growth rate as

$$\sigma_\mathrm{f} = -0.31\,\frac{1}{N_0}\frac{g}{c_p}\left(\frac{\partial s}{\partial y}\right)_p. \tag{9}$$

Figure 2b compares σ_s, where N is computed instantaneously and locally, with σ_f, where we use the optimum value of stability. Statistical comparisons are repeated in Tables 2 and 1, demonstrating that allowing stability to vary does not make a meaningful difference to area mean baroclinicity in the storm track. As such we will treat it as a fixed parameter henceforth, as consistent with the quasigeostrophic framework which underpins the interpretation of the Eady growth rate as a relevant measure for cyclone growth rate.

3 An entropy framework for area mean baroclinicity

Baroclinic instabilities are large scale wave instabilities, growing on a baroclinically unstable background. Smaller scale details in the temperature gradients will modify local values of the Eady growth rate, but we hypothesise they do not play a substantial role in the growth rate of baroclinic waves; these will be sensitive to the larger scale temperature gradients only. Therefore, we are mainly interested in the area mean Eady growth rate, where the area is chosen to contain the strong baroclinic region of the storm track.

The area mean baroclinicity for a geographically confined region A is

$$\overline{\sigma_\mathrm{f}} = \frac{1}{A}\iint_A \sigma\,\mathrm{d}A = -0.31\frac{g}{c_p\,N_0 A}\iint_A \frac{\partial s}{\partial y}\,\mathrm{d}A. \tag{10}$$

Given the integrand is a meridional derivative, we next explore the extent to which we can approximate the integration by omitting the cosine latitude dependence. We can then interpret $\mathrm{d}A$ as the Cartesian measure of area (that is, $\mathrm{d}A = \mathrm{d}x\,\mathrm{d}y$) and use Green's integral theorem (Marsden and Tromba, 1996), to write

$$\overline{\sigma_\mathrm{f}} = 0.31\frac{g}{c_p\,N_0 A}\oint_{\partial A} s\,\mathrm{d}x. \tag{11}$$

where ∂A is the positively oriented boundary of area A, and x is the zonal coordinate. For the southern hemisphere a minus-sign is introduced to this expression.

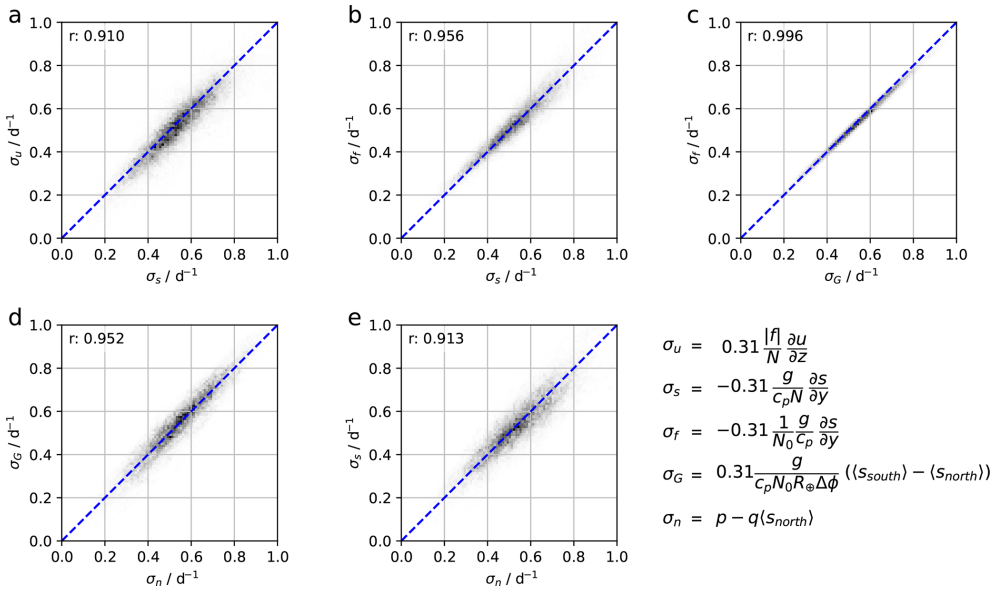

Figure 2. Comparisons of calculation methods of two hourly area average baroclinicity in the storm track region (30 to 50° N, 30 to 80° W) across the 30 winters (DJF) from 1991 to 2021 for 775 hPa. In all plots the 1–1 line is shown in dashed blue. Each plot shows the Eady growth rate calculated with: **(a)** a zonal wind shear dependence (σ_u, Eq. 1), compared with a meridional entropy gradient dependence (σ_s, Eq. 8); **(b)** a meridional entropy gradient dependence (σ_s, Eq. 8), with stability N calculated as Eq. (2), compared with the same equation but where stability is a fixed parameter (σ_f, Eq. 9); **(c)** a meridional entropy gradient dependence with fixed stability (σ_f, Eq. 9), compared with σ_G (Eq. 12) where Green's theorem is applied; **(d)** the Green's theorem version (σ_G, Eq. 12) compared with a linear regression where only $\langle s_{\text{north}} \rangle$ varies (σ_n, Eq. 13); **(e)** a meridional entropy gradient dependence (σ_s, Eq. 8), with stability N as a horizontally varying field compared with a linear regression where only $\langle s_{\text{north}} \rangle$ varies (σ_n, Eq. 13). The table in the bottom right shows the expressions used.

Table 2. Correlations for different forms of the Eady growth rate. A description of the variables is as Table 1.

	σ_u	σ_s	σ_f	σ_G	σ_n	σ_{south}
σ_u (vertical wind shear)	1.00					
σ_s (meridional entropy gradient)	0.91	1.00				
σ_f (σ_s, fixed N)	0.91	0.96	1.00			
σ_G (σ_f, not area mean)	0.91	0.94	0.996	1.00		
σ_n (50° N entropy)	0.86	0.91	0.95	0.95	1.00	
σ_{south} (30° N entropy)	0.41	0.38	0.44	0.38	0.15	1.00

Performing this contour integral over the latitude–longitude box, we find

$$\sigma_G = 0.31 \frac{g}{c_p N_0 R_\oplus \Delta\phi} \left(\langle s_{\text{south}} \rangle - \langle s_{\text{north}} \rangle \right), \tag{12}$$

where $R_\oplus$ is Earth's radius in metres, $\Delta\phi$ is the difference of the latitudinal edges of the integrated region in radians, and s_{south} and s_{north} represent the specific entropy along the meridional borders of the region closest to the equator and pole respectively, with angled brackets denoting the mean across the latitude line.

Using Eq. (12), mean baroclinicity can be calculated for a region with just a rescaling of the difference in specific entropy along its meridional borders. This means that baroclinicity in a region can be enhanced with an increase or decrease in entropy on the equatorward or poleward side of a baroclinic zone respectively; any internal variations in baroclinicity that do not alter these mean boundary values do not contribute to variations in the mean baroclinicity.

Figure 2c compares σ_f with σ_G, the difference being that σ_f uses an area mean and σ_G uses a grid mean where all model cells are considered as having equal area. It is clear visually that applying the Green's theorem makes little difference to the spread of the data. In other words, considering a Cartesian mean rather than the area mean does not change the measure of baroclinicity in any relevant way. The mean, variance, and correlation of these measures can be found in Tables 1 and 2.

Equal changes in entropy along either the north or south border of the storm track have an identical effect on σ_G, though entropy along the north border varies more than to the south, as is shown in Fig. 3. We quantify this difference with their standard deviations over the 30 winter period, be-

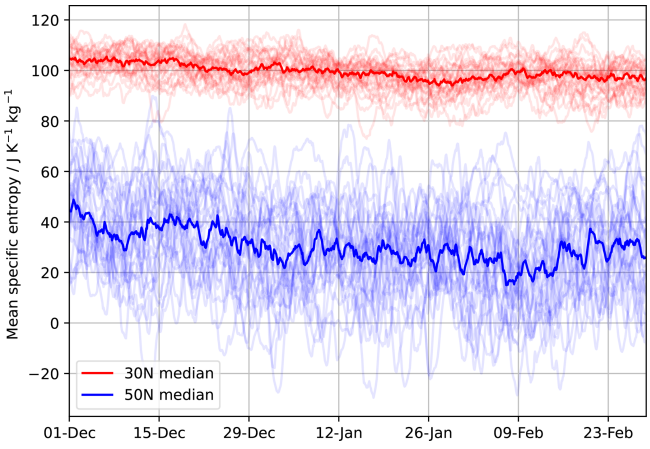

Figure 3. 775 hPa mean specific entropy along the 30 to 80° W latitude line at 30° N (red) and 50° N (blue). Faint lines show individual years in our 30 winter climatology, while bold lines show the median across the climatology. The climatological mean shows a similar patten to the median, except with reduced variability.

ing 6.2 J kg^{-1} K^{-1} for $\langle s_{\text{south}} \rangle$, smaller than that of $\langle s_{\text{north}} \rangle$ which is 18.2 J kg^{-1} K^{-1}. This indicates that the variability in the area mean baroclinicity in the N. Atlantic storm track is mainly determined by processes on its north border.

Figure 3 also shows that there is not a strong seasonal cycle in $\langle s_{\text{south}} \rangle$ relative to variability in $\langle s_{\text{north}} \rangle$, rather $\langle s_{\text{south}} \rangle$ mainly contributes noise to σ_{G}. We can therefore treat $\langle s_{\text{south}} \rangle$ as a constant during winter while preserving much of the variability in σ_{G}. This allows us to express the Eady growth rate, through a linear regression, as dependent on $\langle s_{\text{north}} \rangle$ as its only variable. Performing this linear regression between $\langle s_{\text{north}} \rangle$ and σ_{G} gives the expression

$$\sigma_n = p - q\,\langle s_{\text{north}} \rangle, \quad p = 0.797\,\text{d}^{-1},$$
$$q = 1.0496 \frac{0.31 g}{c_p\, N_0\, R_\oplus\, \Delta\phi}, \tag{13}$$

where p and q are coefficients in the univariate least square fit.

From this linear regression it is clear that entropy along the north boundary of our storm track region is the main factor determining variations in baroclinicity in the region, as the coefficient ahead of the constants in the q term is near 1. The fact that the coefficient is not exactly 1 accounts for the covariability between $\langle s_{\text{north}} \rangle$ and $\langle s_{\text{south}} \rangle$; that this coefficient is slightly above 1 indicates weak negative covariability.

We can compare Eq. (13) with an equivalent where we replace $\langle s_{\text{north}} \rangle$ with $\langle s_{\text{south}} \rangle$ to give σ_{south}, repeating the statistical comparison with Eq. (12) to find that the correlation coefficient decreases from 0.95 to 0.38. Additionally, the standard deviation for σ_{south} decreases to 0.07 d^{-1}, demonstrating its poor similarity to σ_{G} which has a standard deviation of 0.159 d^{-1}. Entropy at the two borders is weakly anti-correlated, with a correlation coefficient between $\langle s_{\text{north}} \rangle$ and $\langle s_{\text{south}} \rangle$ of −0.15. Given $\langle s_{\text{north}} \rangle$ provides a good estimate for area mean baroclinicity, it is unsurprising that $\langle s_{\text{south}} \rangle$, which is uncorrelated with it, is not a good estimator of baroclinicity. This further demonstrates that variability in area mean baroclinicity is linked to processes altering temperature to the north, rather than processes internal to or south of the storm track.

Comparing σ_n with σ_{G} in Fig. 2d demonstrates that by removing any dependence on $\langle s_{\text{south}} \rangle$ the Eady growth rate is not significantly affected numerically. By design of the linear regression, the two expressions share a mean value, 0.55 d^{-1}, but the standard deviation in σ_n is slightly lower, decreasing from 0.159 to 0.151 d^{-1}, showing the weaker variability in entropy to the south and suggesting $\langle s_{\text{south}} \rangle$ was introducing noise rather than a coherent signal contributing to changes in baroclinicity.

As shown, synoptic-timescale variations in area mean baroclinicity are mainly determined by entropy-changing processes on the poleward side of the storm track. Such processes include cold-air outbreaks originating from North America and the Labrador Sea.

In this manipulation of the Eady growth rate, we began with an agreed upon expression with variables $\partial u/\partial z$ and $1/N$ (Eq. 1), applied thermal wind balance to replace the zonal wind shear term with $(\partial s/\partial y)_p$ (Eq. 8), treated the variable $1/N$ as a parameter so $(\partial s/\partial y)_p$ is the only variable (Eq. 9), applied the Green's integration theorem to reduce area mean growth rate to a scaling of the difference in mean entropy between the north and south borders (Eq. 12), and performed a linear regression to express the Eady growth rate with $\langle s_{\text{north}} \rangle$ as its only variable (Eq. 13).

The difference between σ_s and σ_u is entirely physical, because it measures the lack of geostrophic balance in the storm track. In the quasi-geostrophic context, which underpins the physical relevance of the Eady growth rate, the two expressions are equivalent, meaning that we can use the expression σ_s as our benchmark to compare our final result with. Figure 2e compares σ_n with σ_s, demonstrating that these steps, which all introduce moderate numerical differences due to the simplifying choices we made, do not dramatically affect the values of the inferred growth rate. The total change introduced in going from σ_s to σ_n is in fact less than the difference between σ_u and σ_s which are, as discussed, both equally valid forms of the Eady growth rate.

Throughout this work we consider the upstream region of the N. Atlantic storm track well contained in the area 30 to 50° N, 30 to 80° W, focussing largely on the north edge of this area. This box contains the most active region of the storm track, particularly in terms of the genesis of cyclones. We now determine the latitude range for which the linear regression used in Eq. (13) obtains good results.

Figure 4 shows the changing correlation coefficient between σ_{f} and σ_n as the north and south edges of our chosen region are adjusted. The east and west edges of the box are otherwise fixed at 30 and 80° W. For each new latitude pair

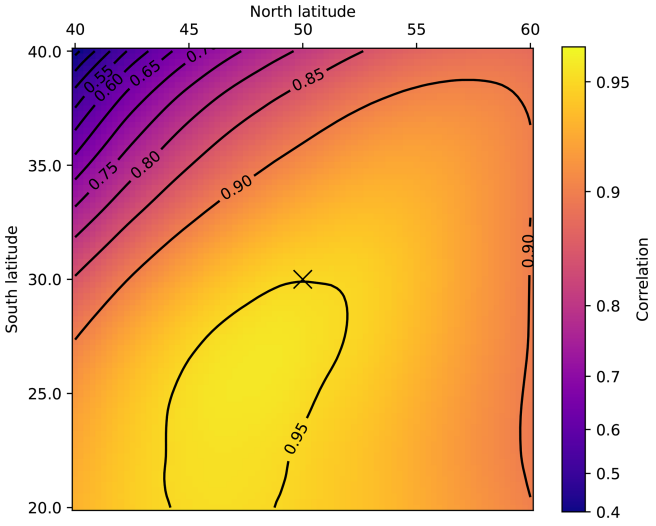

Figure 4. Correlation between 30 winter (DJF) area mean baroclinicity σ_f and $\langle s_{\text{north}} \rangle$ at 775 hPa. The east and west borders of the region are fixed at 30 and 80° W, and the north and south borders vary in the x and y axes respectively, with a cross marker showing 30° N, 50° W. Contours show correlation in linear intervals and colours show it scaled by its Fisher transform (Fisher, 1915).

defining the borders of the region, the optimum stability N_0 is recalculated along with new coefficients in Eq. (13) for the linear regression for σ_n.

The cross marker in Fig. 4 shows the 30, 50° N bounds that we use in our prior analysis, lying just outside the 0.95 correlation coefficient contour. The maximum correlation value, 0.955, is found when the north and south borders are set to 26.25 and 48.25° N. This is barely higher than the 0.950 correlation we find for 30 and 50° N, demonstrating there is a large range of latitudes where the analysis works equally well, shown also by the shading in Fig. 4. Our choice of 30 to 50° N, 30 to 80° W clearly satisfies both motivations in containing the region of climatologically strongest baroclinicity and showing high correlation between σ_n and σ_f.

Interestingly as the borders become close (Fig. 4 top-left) the correlation decreases sharply, the reason for this being as we make the region smaller σ_f effectively give us a mean value of local $\partial s/\partial y$, and there is no reason this should be strongly linked to the magnitude of $\langle s_{\text{north}} \rangle$. It also appears that correlation scales strongly with the domain size for the same reason: all 5° latitude ranges have a correlation coefficient around 0.7, all 10° ranges around 0.85. This behaviour seems limited by the north border, as the correlation begins to decrease as the north latitude goes further than 50° N. For these higher latitudes it seems that the correlation is less dependent on the position of the south border, as the correlation contours vary more as the north latitude increases, that is to say keeping the north border fixed at 50° N but moving the south border from 30 to 20° N leads to very little change in correlation, whereas keeping the south fixed at 30° N and extending the north border to 60° N leads to a more significant decrease in correlation.

It is clear that the relationship described between area mean baroclinicity in the storm track and $\langle s_{\text{north}} \rangle$ is not uniquely found for our specific choice of 30 to 50° N, as there is a wide band of latitudes where the correlation between σ_f and σ_n remains high. This is however not the only reason to choose a latitude range, it is also clearly important that the region contains well the upstream region of the storm track, which 30 to 50° N, 30 to 80° W clearly does.

4 A simple budget for baroclinicity

Our results indicate that a dynamical budget for area mean baroclinicity is actually quite simple: it just requires a temperature tendency equation averaged over the north border of the storm track. To demonstrate practically that Eq. (13) is suitable for such a budget, mean baroclinicity in the N. Atlantic storm track (30–50° N, 30–80° W) over the first winter of our climatology (1991/1992, DJF) is shown in Fig. 5. 10 d Lanczos low and high pass filters have been applied to separate shorter-timescale behaviour from the sub-seasonal trend in baroclinicity, calculated with σ_u (Eq. 1, black), σ_s (Eq. 8, blue), and σ_n (Eq. 13, red), showing there is good agreement in the three expressions at both the long and short timescales. For the longer timescales we see there is no systematic drift between the measures, and for the shorter timescales the main difference emerges around diurnal frequencies, where σ_u shows the largest variance for reasons discussed in section 2, σ_s shows less variance, and σ_n less variance still. The increased variability of σ_s over σ_n is due to the fact that the full area mean entropy gradient form of baroclinicity given by σ_s is dependent on entropy at both the north and south edges of the domain, whereas the linear regression used for σ_n is dependent on only the north edge and therefore has fewer independent sources of variability. In this case σ_n, which shows less high frequency variability, is preferable because high frequency variability in baroclinicity is not relevant to quantifying the growth rate of baroclinic eddies.

Given that σ_u and σ_s are equally valid realisations of baroclinicity, and that the behaviour of σ_n is essentially indistinguishable from them, it is clearly suitable to treat variability in σ_n as variability in baroclinicity.

A budget for baroclinicity is therefore equivalent to a budget for entropy at the north edge of the domain, which is

$$\frac{\partial s}{\partial t} = \frac{q}{T} - \boldsymbol{v} \cdot \nabla s - \omega \left(\frac{\partial s}{\partial p} \right), \tag{14}$$

where $\partial s/\partial t$ represents the entropy tendency, q/T diabatic processes, $\boldsymbol{v} \cdot \nabla s$ the horizontal advection of entropy gradients, and ω $(\partial s/\partial p)$ their vertical advection. In this budget, changes in mean baroclinicity calculated with Eq. (13) scale linearly with $\partial s/\partial t$, and we are therefore able to consider the other terms as sources and sinks of baroclinicity since they

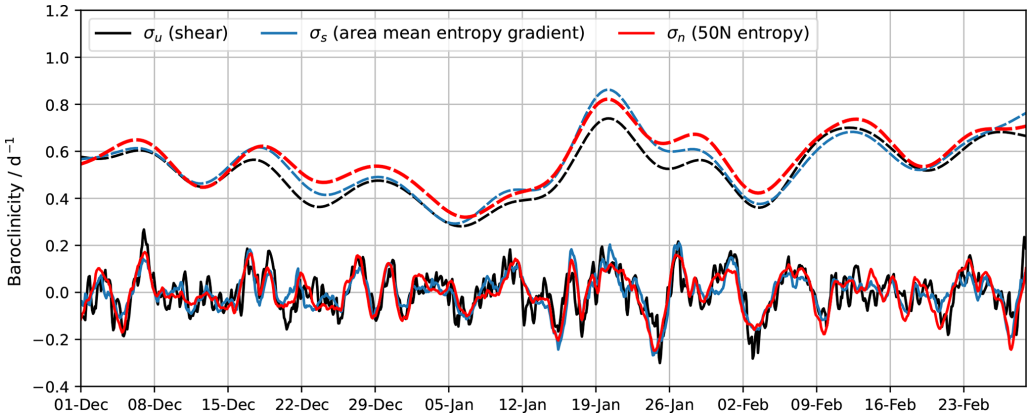

Figure 5. Mean baroclinicity in the region 30–50° N, 30–80° W for winter (DJF) 1991/1992, calculated with σ_s (black), σ_s (blue), and σ_n (red). Low and high pass filters based on a Lanczos filter are applied – in the dashed line a 10 d low pass is applied, and in the solid line a 10 d high pass is applied so that the sum of the two signals adds exactly to the complete signal.

affect the entropy tendency, attributing changes in baroclinicity to the individual terms. A paper on the implications of this budget is currently in preparation.

As we demonstrated, our new expression for area mean baroclinicity, σ_n, depends only on entropy at a single given latitude, so its tendency is only influenced by processes local to that latitude. In comparison to any dynamical budget which required the involvement of processes across a wide area, σ_n provides a very simple means to calculate mean baroclinicity which, being linearly dependent on $\partial s/\partial t$, integrates baroclinicity into our dynamical budget with ease. This means that a complete dynamical budget for baroclinicity in the N. Atlantic storm track only requires data from 50° N and the nearest two latitudes in any dataset to compute $\boldsymbol{v} \cdot \nabla s$, and two equidistant vertical levels to give ω $(\partial s/\partial p)$.

5 Conclusions

We have demonstrated that area averaged Eady growth rate can be rearranged through thermal wind balance to be dependent on a meridional entropy gradient, eliminating much of the high-frequency variation found when it is calculated using zonal wind shear. These oscillations associated with the diurnal cycle do not contribute to the development of baroclinic instabilities, so reducing them provides a more coherent estimation of baroclinicity without requirement of time filtering. This form of baroclinicity, σ_s (Eq. 8), is equally valid as its more common expression, σ_u (Eq. 1), as each are equivalent within the context of the validity of the Eady model used to diagnose growth rates.

The lack of geostrophic balance introduces a difference in values between the two measures. Their common variance is 83 %, suggesting that the quantitative determination of physically relevant area mean baroclinicity has a minimum uncertainty variance of around 17 %; there is no real benefit in improving measures of baroclinicity beyond this uncertainty, because the two physically equivalent measures already have this level of discrepancy.

We have shown that mean baroclinicity in the N. Atlantic storm track can be accurately approximated by a linear regression of mean dry entropy to the north of the storm track, with 83 % of the variability in area mean baroclinicity in our chosen region being captured by $\langle s_{\text{north}} \rangle$. Our data has a 2 h resolution and therefore contains variability of all frequencies up to the Nyquist frequency of 6 d^{-1}. Any time filtering would further enhance this correspondence.

Because the variability of the area mean baroclinicity is well captured by entropy at the north border of the storm track, any processes that modify the temperature field inside the storm track region, such as latent heat release and other frontal effects, only have a bearing on area mean baroclinicity insofar as these processes also modify the mean entropy at the north border. It also means that processes outside the storm track region can modify the area mean baroclinicity as long as these processes also modify the mean entropy at the north border of the storm track. These results may be consistent with those found in Federer et al. (2026), where relevant available potential energy fluxes are found to the north of the storm track.

Data availability. The ERA5 data used for the reanalysis can be freely obtained from the ECMWF Copernicus Climate Change Service (C3S) website (https://doi.org/10.24381/cds.143582cf, Hersbach et al., 2017).

Author contributions. RB and MA conceived of the work. RB performed the data analysis, visualisations, and wrote the work. MA and BH gave scientific advice and suggestions for the written work.

Competing interests. The contact author has declared that none of the authors has any competing interests.

Disclaimer. Publisher's note: Copernicus Publications remains neutral with regard to jurisdictional claims made in the text, published maps, institutional affiliations, or any other geographical representation in this paper. The authors bear the ultimate responsibility for providing appropriate place names. Views expressed in the text are those of the authors and do not necessarily reflect the views of the publisher.

Acknowledgements. We thank three anonymous reviewers whose comments helped improve the manuscript and who suggested the new analysis in Sect. 4 and Figs. 4 and 5.

Financial support. This research has been supported by the Natural Environment Research Council (SCENARIO DTP grant NE/S007261/1).

Review statement. This paper was edited by Nili Harnik and reviewed by three anonymous referees.

References

Ambaum, M. H. P. and Novak, L.: A nonlinear oscillator describing storm track variability, Q. J. Roy. Meteor. Soc., 140, 2680–2684, https://doi.org/10.1002/qj.2352, 2014.

Binder, H., Boettcher, M., Joos, H., and Wernli, H.: The Role of Warm Conveyor Belts for the Intensification of Extratropical Cyclones in Northern Hemisphere Winter, J. Atmos. Sci., 73, 3997–4020, https://doi.org/10.1175/JAS-D-15-0302.1, 2016.

Blackmon, M. L., Wallace, J. M., Lau, N.-C., and Mullen, S. L.: An Observational Study of the Northern Hemisphere Wintertime Circulation, J. Atmos. Sci., 34, 1040–1053, https://doi.org/10.1175/1520-0469(1977)034<1040:AOSOTN>2.0.CO;2, 1977.

Bretherton, F. P.: Baroclinic instability and the short wavelength cut-off in terms of potential vorticity, Q. J. Roy. Meteor. Soc., 92, 335–345, https://doi.org/10.1002/qj.49709239303, 1966.

Eady, E. T.: Long Waves and Cyclone Waves, Tellus, 1, 33–52, https://doi.org/10.1111/j.2153-3490.1949.tb01265.x, 1949.

Federer, M., Le May, S., Sprenger, M., and Papritz, L.: Collapses of Hemispheric Available Potential Energy, Geophys. Res. Lett., 53, e2025GL119424, https://doi.org/10.1029/2025GL119424, 2026.

Fisher, R. A.: Frequency Distribution of the Values of the Correlation Coefficient in Samples from an Indefinitely Large Population, Biometrika, 10, 507–521, https://doi.org/10.2307/2331838, 1915.

Hersbach, H., Bell, B., Berrisford, P., Hirahara, S., Horányi, A., Muñoz-Sabater, J., Nicolas, J., Peubey, C., Radu, R., Schepers, D., Simmons, A., Soci, C., Abdalla, S., Abellan, X., Balsamo, G., Bechtold, P., Biavati, G., Bidlot, J., Bonavita, M., De Chiara, G., Dahlgren, P., Dee, D., Diamantakis, M., Dragani, R., Flemming, J., Forbes, R., Fuentes, M., Geer, A., Haimberger, L., Healy, S., Hogan, R.J., Hólm, E., Janisková, M., Keeley, S., Laloyaux, P., Lopez, P., Lupu, C., Radnoti, G., de Rosnay, P., Rozum, I., Vamborg, F., Villaume, S., and Thépaut, J.-N.: Complete ERA5 from 1940: Fifth generation of ECMWF atmospheric reanalyses of the global climate, Copernicus Climate Change Service (C3S) Data Store (CDS) [data set], https://doi.org/10.24381/cds.143582cf, 2017.

Hersbach, H., Bell, B., Berrisford, P., Hirahara, S., Horányi, A., Muñoz-Sabater, J., Nicolas, J., Peubey, C., Radu, R., Schepers, D., Simmons, A., Soci, C., Abdalla, S., Abellan, X., Balsamo, G., Bechtold, P., Biavati, G., Bidlot, J., Bonavita, M., De Chiara, G., Dahlgren, P., Dee, D., Diamantakis, M., Dragani, R., Flemming, J., Forbes, R., Fuentes, M., Geer, A., Haimberger, L., Healy, S., Hogan, R. J., Hólm, E., Janisková, M., Keeley, S., Laloyaux, P., Lopez, P., Lupu, C., Radnoti, G., de Rosnay, P., Rozum, I., Vamborg, F., Villaume, S., and Thépaut, J.-N.: The ERA5 global reanalysis, Q. J. Roy. Meteor. Soc., 146, 1999–2049, https://doi.org/10.1002/qj.3803, 2020.

Hoskins, B. J. and James, I. N.: Fluid Dynamics of the Midlatitude Atmosphere, Chap. 5, John Wiley & Sons, Ltd, ISBN 9781118526002, https://doi.org/10.1002/9781118526002, 2014.

Hoskins, B. J. and Valdes, P. J.: On the Existence of Storm-Tracks, J. Atmos. Sci., 47, 1854–1864, https://doi.org/10.1175/1520-0469(1990)047<1854:OTEOST>2.0.CO;2, 1990.

Hotta, D. and Nakamura, H.: On the Significance of the Sensible Heat Supply from the Ocean in the Maintenance of the Mean Baroclinicity along Storm Tracks, J. Climate, 24, 3377–3401, https://doi.org/10.1175/2010JCLI3910.1, 2011.

James, I. N.: Introduction to Circulating Atmospheres, Cambridge Atmospheric and Space Science Series, Cambridge University Press, https://doi.org/10.1017/CBO9780511622977, 1994.

Lindzen, R. S. and Farrell, B.: A Simple Approximate Result for the Maximum Growth Rate of Baroclinic Instabilities, J. Atmos. Sci., 37, 1648–1654, https://doi.org/10.1175/1520-0469(1980)037<1648:ASARFT>2.0.CO;2, 1980.

Lorenz, E. N.: Available Potential Energy and the Maintenance of the General Circulation, Tellus, 7, 157–167, https://doi.org/10.1111/j.2153-3490.1955.tb01148.x, 1955.

Marcheggiani, A. and Ambaum, M. H. P.: The role of heat-flux–temperature covariance in the evolution of weather systems, Weather Clim. Dynam., 1, 701–713, https://doi.org/10.5194/wcd-1-701-2020, 2020.

Marsden, J. E. and Tromba, A. J.: Vector Calculus, 4th edn., W. H. Freeman and Company, ISBN 0716724324, 1996.

Novak, L., Ambaum, M. H. P., and Tailleux, R.: The Life Cycle of the North Atlantic Storm Track, J. Atmos. Sci., 72, 821–833, https://doi.org/10.1175/JAS-D-14-0082.1, 2015.

Papritz, L. and Spengler, T.: Analysis of the slope of isentropic surfaces and its tendencies over the North Atlantic, Q. J. Roy. Meteor. Soc., 141, 3226–3238, https://doi.org/10.1002/qj.2605, 2015.

Pinto, J. G., Gómara, I., Masato, G., Dacre, H. F., Woollings, T., and Caballero, R.: Large-scale dynamics associated with clustering of extratropical cyclones affecting Western Europe, J. Geophys. Res.-Atmos., 119, 13704–13719, https://doi.org/10.1002/2014JD022305, 2014.

Rodwell, M. J., Magnusson, L., Bauer, P., Bechtold, P., Bonavita, M., Cardinali, C., Diamantakis, M., Earnshaw, P., Garcia-

Mendez, A., Isaksen, L., Källén, E., Klocke, D., Lopez, P., McNally, T., Persson, A., Prates, F., and Wedi, N.: Characteristics of Occasional Poor Medium-Range Weather Forecasts for Europe, B. Am. Meteorol. Soc., 94, 1393–1405, https://doi.org/10.1175/BAMS-D-12-00099.1, 2013.

Schemm, S. and Rivière, G.: On the Efficiency of Baroclinic Eddy Growth and How It Reduces the North Pacific Storm-Track Intensity in Midwinter, J. Climate, 32, 8373–8398, https://doi.org/10.1175/JCLI-D-19-0115.1, 2019.

Simmons, A. J. and Hoskins, B. J.: The Downstream and Upstream Development of Unstable Baroclinic Waves, J. Atmos. Sci., 36, 1239–1254, https://doi.org/10.1175/1520-0469(1979)036<1239:TDAUDO>2.0.CO;2, 1979.

Valdes, P. J. and Hoskins, B. J.: Baroclinic Instability of the Zonally Averaged Flow with Boundary Layer Damping, J. Atmos. Sci., 45, 1584–1593, https://doi.org/10.1175/1520-0469(1988)045<1584:BIOTZA>2.0.CO;2, 1988.

Weijenborg, C. and Spengler, T.: Diabatic Heating as a Pathway for Cyclone Clustering Encompassing the Extreme Storm Dagmar, Geophys. Res. Lett., 47, https://doi.org/10.1029/2019GL085777, 2020.

Zappa, G., Shaffrey, L. C., Hodges, K. I., Sansom, P. G., and Stephenson, D. B.: A Multimodel Assessment of Future Projections of North Atlantic and European Extratropical Cyclones in the CMIP5 Climate Models, J. Climate, 26, 5846–5862, https://doi.org/10.1175/JCLI-D-12-00573.1, 2013.